RSC Advances

ROYAL SOCIETY OF CHEMISTRY

www.rsc.org/advances

Cite this: DOI: 10.1039/c0xx00000x

www.rsc.org/xxxxxx

ARTICLE TYPE

Sol-gel hydrothermal synthesis of microstructured CaO-based adsorbents for CO_2 capture

Nwe Ni Hlaing[a,b,c], Srimala Sreekantan*[a], Radzali Othman[a], Swee-Yong Pung[a], Hirofumi Hinode*[b], Winarto Kurniawan[b], Aye Aye Thant[c], Abdul Rahman Mohamed[d], Chris Salime[e]

Received (in XXX, XXX) Xth XXXXXXXXX 20XX, Accepted Xth XXXXXXXXX 20XX
DOI: 10.1039/b000000x

In this study, microstructured CaO-based adsorbents were synthesized by a sol–gel hydrothermal method using calcium nitrate tetrahydrate, citric acid and sodium hydroxide as precursors. Experiments with different NaOH concentrations (2, 6 and 10 M) were carried out to investigate the effects on the morphologies and CO_2 adsorption activities of the synthesized adsorbents. X–ray diffraction (XRD) and field–emission scanning electron microscopy (FESEM) results showed that different NaOH concentrations resulted in different crystal phases and morphologies. The novel three–dimensional (3D) hierarchical calcite ($CaCO_3$) hollow microspherical adsorbent composed of one–dimensional (1D) spike–shaped nanorods was obtained with 2 M NaOH. XRD analyse confirmed that the hierarchical $CaCO_3$ hollow microspheres were characteristic of the calcite phase. The FESEM image revealed that the microspheres were composed of 1D spike–shaped nanorods with an average length of 500 nm. The cross–sectional FESEM image showed that the microspheres had hollow structures with an average inner cavity of 2 μm and shell thickness of approximately 0.5μm. The CO_2 adsorption performances of the synthesized adsorbents were investigated using a thermogravimetry–differential thermal analysis (TG–DTA) apparatus. Results indicated that the novel hierarchical calcite ($CaCO_3$) hollow microspherical adsorbent composed of one–dimensional (1D) spike–shaped nanorods possessed higher carbonation conversion of 45% after 15 cycles, which was about 22% higher than that of other adsorbents synthesized with 6 and 10 M NaOH concentration and limestone. This property could be attributed to the 3D hierarchical hollow microsphere structure, 1D spike–shaped nanorod structure, trimodal pore size distribution and large BET surface area (44.85 m^2/g) of the novel adsorbent.

1. Introduction

In recent years, three–dimensional (3D) hierarchical hollow microspheres composed of one–dimensional (1D) nanostructures have extensively attracted attention because of their well–defined morphology, low density, large surface area and high performance. These properties enable a wide range of potential applications, such as in adsorption and separation, energy conversion, electronics, optoelectronics, catalysis, sensors and drugs delivery.[1-3] Therefore, various types of materials such as In_2O_3,[4] SnO_2,[5] hydroxyapatite,[6] V_2O_5,[7] β–$Ni(OH)_2$,[8] ZnO,[9] $TiOSO_4$,[10] MnO_2,[11] CuO,[12] α–Fe_2O_3[13] and $CaCO_3$[14-19] hierarchical hollow microspheres have been prepared by different synthesis methods such as hydrothermal, precipitation, solvothermal, mixing and gas–diffusion methods. Their applications in various fields are summarized in Table 1. Among these synthesis methods, hard and soft templates approaches are favourable for the formation of hollow spheres.[1-19] However, hollow spheres prepared using the hard template route usually possess disadvantages related to high cost and tedious synthetic procedures such as rinsing and calcination or chemical etching to remove the templates; which not only destroys the core–shell structures, but is also time and energy–consuming. In addition, the size and morphology of the final hollow spheres mainly depend on the templates (e.g., SiO_2 carbon spheres, polymers).[20, 21] Using the soft template (e.g., micelles, ionic liquid) route is relatively easier, however, large quantities of surfactants or functionalized organic acids are required. Moreover, the shape, shell thickness, and diameter distribution of the resulting hollow particles are difficult to control because of the deformability of the soft templates.[1, 21, 22] In other words, both methods possess some disadvantages. Therefore, it is highly desirable to develop a new approach without templates for the preparation of 3D hierarchical hollow microspheres assembled by 1D nanostructure materials.

Calcium carbonate is one of the most abundant natural minerals found in different polymorphs: three anhydrous crystalline polymorphs (calcite, aragonite, and vaterite) and three metastable forms (amorphous calcium carbonate (ACC), crystalline hexahydrate and crystalline monohydrate).[23, 24] Hierarchical $CaCO_3$ hollow microspheres are attracting significant interest because of their excellent properties such as low density, high surface areas, and their potential application in industry (e.g., filler and coating pigment)[19] and health care (e.g.,

Cite this: DOI: 10.1039/c0xx00000x

www.rsc.org/xxxxxx

ARTICLE TYPE

Table 1 Summary of different types of hierarchical hollow microspheres and their applications.

Samples	Templates / additives / solvents	Method	Application	Ref
In_2O_3	ethylenediamine	hydrothermal	gas sensors	4
SnO_2	sulfonated polystyrene hollow spheres	hydrothermal	anode materials for lithium–ion batteries	5
Hydroxyapatite	polyaspartic acid	hydrothermal	water treatment	6
V_2O_5	polyvinylpyrrolidone and ethylene glycol	mixing	cathode material in lithium–ion batteries	7
β-$Ni(OH)_2$	urea	hydrothermal	–	8
ZnO	pluronic P123 and hexamethylenetetramine	solvothermal	–	9
$TiOSO_4$	glycerol and ethanol	solvothermal	photocatalytic	10
MnO_2	ethanol	mixing	waste–water treatment	11
CuO	–	hydrothermal	anode materials for lithium ion batteries	12
α–Fe_2O_3	glycerol–quasiemulsion microdroplets	hydrothermal	anode materials for lithium–ion batteries	13
$CaCO_3$	polyvinylpyrrolidone and sodium dodecyl sulfonate	precipitation	–	14
$CaCO_3$	carboxyl–terminated hyperbranched polyglycerol	gas diffusion	–	15
$CaCO_3$	low methoxy pectin	precipitation	–	16
$CaCO_3$	soluble starch	mixing	anticancer drug carrier	17
$CaCO_3$	poly (ethylene oxide)–block–poly (methacrylic acid) and sodium dodecylsulfate	–	–	18
$CaCO_3$	polyoxyet hylene sorbitan monooleate	interfacial reaction	filler and coating pigment	19

anticancer drug carrier).[17] Zhao and Wang [14] synthesized hollow $CaCO_3$ microspheres by the precipitation method employing polyvinylpyrrolidone with sodium dodecyl sulfonate as template for the controlled growth of hollow spheres. Butler et al.[16] reported that low methoxy pectin played a key role in the formation of hollow shells of $CaCO_3$. In 2008, Wei et al.[17] reported the formation of hierarchical $CaCO_3$ hollow microspheres using a soluble starch for anticancer drugs carriers. This application could be attributed to the biocompatibility, biodegradability, and pH–sensitive properties of $CaCO_3$ hollow microspheres. Moreover, Enomae and Tsujino[19] fabricated $CaCO_3$ hollow spheres with polyoxyethylene sorbitan monooleate using the interfacial reaction method. They proposed $CaCO_3$ hollow spheres to be used as a filler and paper coating pigment because hollow structure scatters more light, resulting to high brightness and opacity. According to literatures, the hierarchical $CaCO_3$ hollow microspheres were mostly prepared using templates or additives, which lead to complicated synthesis procedures. These procedures are time and energy consuming, require toxic raw materials, produce pollutants from the removal of the templates and are costly. Therefore, an economical and environmental–friendly template–free synthesis method must be developed to fabricate $CaCO_3$ hollow spheres from the scientific research and practical application point of view.[25, 26] To the best of our knowledge, no studies have been reported on the synthesis of 3D hierarchical calcite $CaCO_3$ hollow microspherical adsorbent composed of one–dimensional (1D) spike–shaped nanorods for CO_2 capture using the sol–gel hydrothermal method. Furthermore, most of these literatures focused on the hierarchical $CaCO_3$ hollow microspheres as smart carriers for anticancer drugs, filler, and coating pigment, but not so much on CO_2 capture.

To capture CO_2 from power plants or industrial processes, several kinds of adsorbents and absorbents (such as amines, zeolite, activated carbon, metal organic framework and calcium oxide) have been investigated.[27] Currently, absorption mainly uses aqueous amine compounds (e.g., monoethanolamine (MEA) and diethanolamine (DEA)) is a commercialized technology for CO_2 separation due to their selectivity for acidic gases and fast reactivity.[28] However, this technique has some of major drawbacks such as high solvent regeneration cost, low CO_2 loading capacity and high equipment corrosion rate.[29] In recent years, calcium oxide based adsorbents are one of the most promising adsorbents to capture CO_2 due to their high adsorption capacity (0.786 g-CO_2/g-adsorbent), wide availability in natural minerals (e.g. limestone and dolomite) and reversible carbonation/calcination reaction.[27] However, the main disadvantage of using CaO adsorbents is the rapid decay in adsorbent performance during multiple cycles because of sintering during every calcination step.[30] In general, the carbonation conversion of the CaO adsorbent derived from limestone is about 80% for the initial cycle and sharply drops to about 25% after 10 cycles.[31, 32] Therefore, thermal precalcination,[33] modification[34] and steam hydration[35] of limestones and synthetic CaO-based adsorbents [36-39] have been proposed to improve the CO_2 adsorption performance.

Herein, we firstly report a 3D hierarchical calcite $CaCO_3$ hollow microspherical adsorbent composed of one–dimensional (1D) spike–shaped nanorods for CO_2 capture synthesized by a sol gel hydrothermal method. The effects of NaOH concentration on the structural properties as well as CO_2 adsorption performance of synthesized adsorbents were studied in detail. The experimental results indicated that the 3D hierarchical calcite $CaCO_3$ hollow microspherical adsorbent composed of one–dimensional (1D) spike–shaped nanorods could be obtained

at 2 M NaOH concentration using hydrothermal reaction. This novel structure exhibited higher carbonation conversion of 45% after 15 cycles, which was about 22% higher than that of other adsorbents synthesized with 6 and 10 M NaOH concentration and limestone.

2. Materials and methods

2.1 Sol–gel hydrothermal synthesis

All reagents used were of analytical grade and were used without further purification. First, dry gel was prepared by the sol–gel method. An equal molar ratio (1:1) of calcium nitrate tetrahydrate ($Ca(NO_3)_2.4H_2O$, R&M chemical) and citric acid monohydrate ($C_6H_8O_7.H_2O$, Merck) was dissolved in 100 ml distilled water. The solution was evaporated by heating at 80 °C on a hot plate with vigorous stirring for 5 h. As water evaporated, the solution became viscous and finally formed a very viscous pale yellow gel. The obtained viscous gel was then dried overnight in an oven at 140 °C.[40, 41] After which, 2 g of dry gel was dissolved into a 2 M NaOH solution and the mixture was stirred for 30 min. Then the stirred mixture was placed in a Teflon–lined stainless–steel autoclave. Hydrothermal reaction was conducted at 170 °C for 16 h. After the hydrothermal reaction, the precipitates were centrifuged, washed several times with distilled water and ethanol, and then dried in an oven at 70 °C for 24 h to obtain the final adsorbent. To investigate the effects of NaOH concentration on the structural properties and CO_2 adsorption capacities, experiments with 6 and 10 M NaOH concentration were carried out under similar conditions. For further comparison, commercial limestone ($CaCO_3$) from Malaysia was used in this study.

2.2 Characterization

The crystal structures of the as–synthesized adsorbents were characterized by X–ray diffraction (XRD) using a Rigaku X–Ray Diffractometer with Cu Kα_1 radiation (λ= 0.154056 nm); the working current and voltage were 20 mA and 40 kV, respectively. The surface morphology of the adsorbents was observed under a S–4700 (Hitachi) field–emission scanning electron microscope (FESEM). The resulting $CaCO_3$ hollow spheres were crosscut using an argon ion beam (Cross Section Polisher (CP) SM–09010, JEOL) and the cross sectional FESEM images were obtained using a S–4700 (Hitachi, FESEM). The samples were coated with a thin layer of platinum to avoid sample charge up before FESEM analysis. The presence of the functional groups (CO_3^{2-}, OH^-) was determined using a JASCO FT/IR–6100 FV Fourier–transform infrared spectroscopy (FTIR) over the region of 400–4,000 cm^{-1} with the KBr pellet technique having spectral resolution of 4 cm^{-1}. A thermogravimetry –differential thermal analysis (TG–DTA) was carried out using a Rigaku TG–DTA. The adsorbents were placed in a platinum crucible and heated at the rate of 10 °C/min up to 900 °C, under N_2 purge at a flow rate of 40 mL/min. Al_2O_3 was used as reference material. The pore structure parameters of the adsorbents were determined from nitrogen adsoption–desorption isotherms using the Quantachrome (Autosorb–1–MP) instrument and the Brunauer–Emmett–Teller (BET) method was used for surface area calculation.

2.3 CO_2 carbonation–calcination performances

To measure the CO_2 adsorption, a Rigaku thermogravimetry –differential thermal analysis (TG–DTA) apparatus with Thermoplus 2 software was used. Carbonation/ calcination processes were performed at 800 °C. A small amount of the adsorbent (~ 6.5 mg) was placed in a platinum crucible and was heated from room temperature to 800 °C at a heating rate of 10 °C/min under 100% N_2 gas flow and atmospheric pressure, and then the temperature was held for 6 min to achieve complete decomposition. Subsequently, carbonation performance was carried out for 30 min under 100% CO_2 gas flow. After the 30 min carbonation process, 100% N_2 gas was flowed for 6 min to calcine the carbonated adsorbent. To investigate the CO_2 adsorption capacity and cyclic stability of the adsorbents, the carbonation/calcination performance was repeated for multiple cycles. The constant flow rate for CO_2 and N_2 gas was 40 ml/min. The CO_2 adsorption capacity and CO_2 conversion were calculated using the following equations;

$$CO_2\ adsorption\ capacity,\ C = \frac{W_N - W_I}{W_I} \quad (1)$$

$$CO_2\ Conversion,\ X_N\ (\%) = \frac{W_N - W_I}{W_I} \times \frac{M_{CaO}}{M_{CO_2}} \times 100 \quad (2)$$

where C is the CO_2 adsorption capacity, X_N is the carbonation conversion, W_N is the weight (%) of the carbonated adsorbents after N cycle(s), W_I is the initial weight (%) of the calcined adsorbents, M_{CaO} and M_{CO_2} are molar masses of CaO and CO_2, respectively.

3. Results and Discussion

3.1 Structure and morphology

Fig. 1(a) shows the X–ray diffraction (XRD) pattern of hierarchical $CaCO_3$ hollow microspherical adsorbent with a rhombohedral phase calcite (JCPDS–05–0586) with R–3c(167) space group.[42] No diffraction peaks related to other impurities was detected. The peak at 2θ = 29.40°, assigned to the (104) plane showed the strongest diffraction which could be assumed

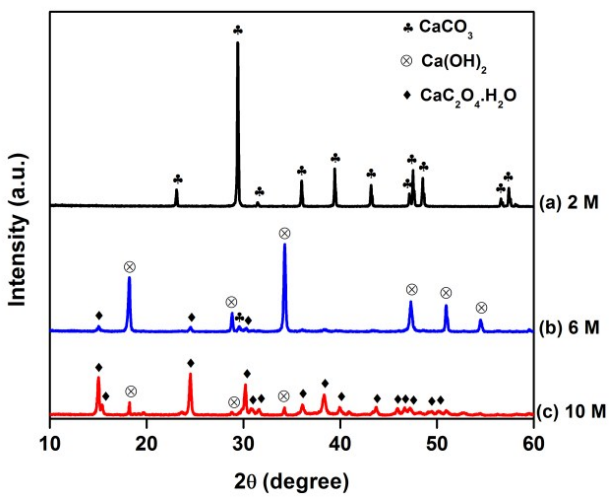

Fig.1 XRD patterns of microstructured CaO-based adsorbents.

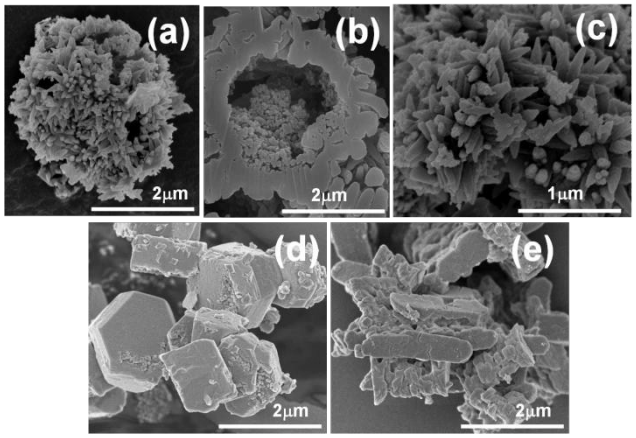

Fig.2 FESEM images of microstructured CaO-based adsorbents: (a) microsphere (b) cross sectional and (c) higher magnification images of 3D hierarchical $CaCO_3$ hollow microspherical adsorbent composed of 1D spike–shaped nanorods, (d) hexagonal and rectangular–shaped $Ca(OH)_2$ and (e) plate–shaped $CaC_2O_4.H_2O$ adsorbents.

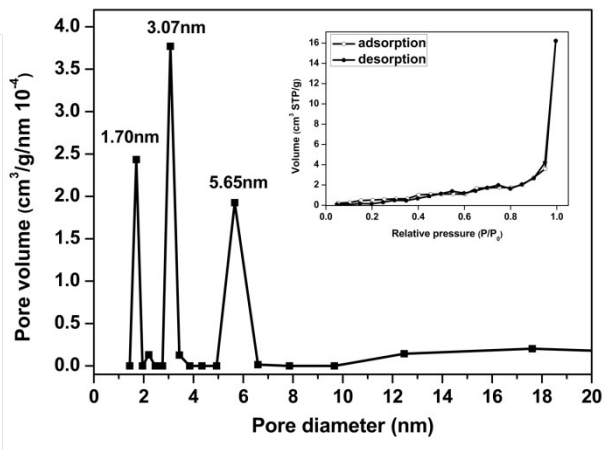

Fig.3 Pore size distribution and N_2–adsorption/desorption isotherm (inset) of 3D hierarchical $CaCO_3$ hollow microspherical adsorbent composed of 1D spike–shaped nanorods.

that $CaCO_3$ grows mainly along the (104) plane, which was in agreement with the XRD pattern of limestone, common $CaCO_3$ (Fig. S1 (ESI†)).Obviously, highly crystallized $CaCO_3$ crystals could be observed under mild hydrothermal condition without calcination at high temperature. The crystallite size calculated using Scherrer equation ($D=0.9\lambda/\beta\cos\theta$) was 76.75 nm.

Fig. S2 (ESI†) shows the FTIR spectrum of the hierarchical calcite $CaCO_3$ hollow microspheres. The characteristic bands of calcite $CaCO_3$ at 711, 874 and 1423 cm^{-1} could be observed in Fig. S2 (ESI†).[43] The broad band observed at 3456 cm^{-1} corresponded to the stretching vibration mode of O–H bond and due to the absorbed water on the surface of the 1D spike–shaped nanorods. The strong and wide band at 1423 cm^{-1} attributed to the asymmetric stretching vibration of the C–O bond while the sharp bands at 874 and 711 cm^{-1} corresponded to the in–plane and out–of–plane bending modes of CO_3^{2-}, respectively.[42]

Fig. 2(a) shows the FESEM image of hierarchical calcite $CaCO_3$ hollow microsphere with an average diameter of 3.3 μm composed of an array of spike–shaped $CaCO_3$ nanorods. The nanorods have grown radially on the surface of the sphere. Fig. 2(b) shows the cross sectional FESEM image of the $CaCO_3$ hollow sphere with an average inner cavity of 2 μm. The inner part of hollow structures was found to comprise particles with several nanometers. The shell thickness of the $CaCO_3$ hollow sphere was about 0.5 μm. Additional detail high magnification structural features are shown in Fig. 2(c). The spike–shaped $CaCO_3$ nanorods had a root size of 110–150 nm and a tip size of 50–70 nm with an average length of 500 nm. The average atomic percentage (at%) of the elements in the $CaCO_3$ hollow spheres was determined using EDX analysis. The EDX spectrum (Fig. S3 (ESI†)) proved that the composition of the hierarchical hollow microsphere adsorbent was pure $CaCO_3$. The pure $CaCO_3$ hollow spheres were composed of 19.96 at% Ca, 27.71 at% C, and 52.33 at% C. The Pt peaks in the EDX spectrum was due to the plated platinum. The FESEM image of the commercial limestone ($CaCO_3$) was shown in Fig. S4 (ESI†).

Fig. 3 shows the trimodal pore size distribution of hierarchical calcite $CaCO_3$ hollow microspherical adsorbent. The first pore size peak was 1.70 nm, which corresponded to the micro–pores, while pore sizes of 3.07 and 5.65 nm corresponded to meso–pores. The N_2– adsorption/desorption isotherm of the hierarchical $CaCO_3$ hollow spheres (inset Fig) was classified as type II isotherm (no plateau at high P/Po) according to the International Union of Pure and Applied Chemistry (IUPAC) classification.[44-46] The BET surface area of the $CaCO_3$ hollow microspheres was 44.85 m^2/g, which was higher than that of the commercial limestone (1.38 m^2/g) and others $CaCO_3$ adsorbents reported in literature such as $CaCO_3$ nanopod (10.40 m^2/g),[37] commercial microsized $CaCO_3$ (12.40 m^2/g) and nanosized $CaCO_3$ (17.00 m^2/g).[47] High surface area has been reported to enhance the CO_2 adsorption capacity and cyclic stability of the adsorbent.[48] The larger BET surface area (44.85 m^2/g) together with the micro–pore and meso–pore size distributions suggested that as–synthesized calcite $CaCO_3$ hollow spheres would exhibit good CO_2 adsorption capacity.

Thermal analysis was carried out to investigate the thermal decomposition temperature of the $CaCO_3$ adsorbent. The TG and DTA curves of the $CaCO_3$ hollow microspheres are shown in Fig. S5 (ESI†). The wide endothermic peak at 779 °C, which coincided with the TG weight loss in the temperature range of 715–795 °C, represented the thermal decomposition of $CaCO_3$ into CaO. Based on this data, the calcination temperature of the hierarchical calcite $CaCO_3$ hollow spheres for multiple cycles were fixed at 800 °C. Results will be discussed in the later section.

3.2 Effect of NaOH concentration

The NaOH concentration was increased from 2 M to 6 and 10 M to investigate the effects of NaOH concentration on the structural properties and CO_2 adsorption performances. As discussed previously, using 2M NaOH resulted in $CaCO_3$. With increased concentration to 6 M NaOH, $Ca(OH)_2$ (calcium hydroxide, JCPDS–78–0315) with a hexagonal phase was observed (Fig. 1(b)). In addition, the presence of minor peaks, which belong to the $CaCO_3$ and $CaC_2O_4•H_2O$ were found. When the concentration of NaOH was further increased to 10 M, a monoclinic phase $CaC_2O_4•H_2O$ (whewellite, JCPDS–20–0231) was obtained (Fig. 1(c)). Some minor peaks at 2θ values of 18.23°, 28.84°, and 34.23° displayed the coexistence of $Ca(OH)_2$ with $CaC_2O_4•H_2O$. Crystallite sizes and BET surface areas of the

synthesized adsorbents are summarized in Table S1 (ESI†).

FTIR spectra were recorded to exhibit the chemical groups of each adsorbent with different NaOH concentrations. The characteristic band of $Ca(OH)_2$ could be seen at 3643 cm^{-1} which represented the O–H stretching mode (Fig. S6(a) (ESI†)).[49] Moreover, the bands at 781, 1318, and 1623 cm^{-1} as well as 874, 1428 cm^{-1}, proved that $CaC_2O_4•H_2O$ and $CaCO_3$ coexist, respectively. In Fig. S6 (ESI†), the sharp band at 1318 cm^{-1} and the strong band at 1618 cm^{-1} attributed to symmetric metal–carboxylate and antisymmetric carbonyl stretching C=O modes, which corresponded to the characteristic bands of $CaC_2O_4•H_2O$.[50, 51] In Fig. S6(b) (ESI†), the weak band at 3642 cm^{-1} signified the existence of $Ca(OH)_2$. In summary, the FTIR spectra are in agreement with the XRD patterns.

The morphology and size of the adsorbents were examined using FESEM. Fig. 2(d) and (e) show the representative FESEM images of the synthesized adsorbents with 6 and 10 M NaOH. Notably, different NaOH concentrations led to the formation of different morphologies. As shown in Fig. 2(d), hexagonal–shaped microstructures with an average size of 1.6 µm and rectangular–shaped microstructures with the length of 1–1.3 µm and the width range from 0.6 to 1 µm were obtained at 6 M NaOH. Fig. 2(e) shows the morphology of the adsorbent obtained at 10 M NaOH. The microplates adsorbent with the length of 2–2.5 µm and the width range from 0.7–1.2 µm was formed under this condition. Fig. S7 (ESI†) shows the EDX spectra of the $Ca(OH)_2$ and $CaC_2O_4•H_2O$ adsorbents. EDX results identified that the composition of the adsorbents was Ca, C and O. For $Ca(OH)_2$ adsorbent Fig. S7(a) (ESI†), the C peak at 0.27 KeV could be attributed to the content of $CaCO_3$ and $CaC_2O_4•H_2O$.

The TG–DTA curves of the $Ca(OH)_2$ and $CaC_2O_4•H_2O$ adsorbents synthesized with 6 and 10 M NaOH are shown in Fig. S8 (ESI†). Weight losses in the TG curves occurred in three stages (Fig. S8(a) and (b) (ESI†)). However, different adsorbents ($Ca(OH)_2$ and $CaC_2O_4•H_2O$) resulted to different weight losses. This might be due to the different amounts of H_2O, CO, and CO_2 in the adsorbents. The first stage of weight loss (100–160 °C) in Fig. S8(a) (ESI†) represented the evolution of water molecule from the small amount of $CaC_2O_4•H_2O$ phase present in the adsorbent. The second weight loss in the temperature range (370–440 °C) represented the dehydroxylation of $Ca(OH)_2$.[52, 53] The final weight loss (560–700 °C) was related to the thermal decomposition of the content of $CaCO_3$ in the $Ca(OH)_2$ adsorbent. In Fig. S8(b) (ESI†), the first stage of significant weight loss (100–190 °C) corresponded to the removal of water molecule from $CaC_2O_4•H_2O$ ($CaC_2O_4•H_2O$ to CaC_2O_4). The second stage (390–510 °C) was related to the evolution of carbon monoxide (CaC_2O_4 to $CaCO_3$) and the final weight loss (770–830 °C) could be attributed to the liberation of CO_2 ($CaCO_3$ to CaO), respectively.[54] The TG weight losses (%) of synthesized adsorbents aer listed in Table S2 (ESI†). The experimental weight losses were lower than the theoretical value for the adsorbents synthesized at 6 and 10 M, because of the presence of different types of impurity phases in the adsorbents.

In Fig. S8(c) (ESI†), the sharp endothermic peak at 423 °C represented the decomposition of $Ca(OH)_2$. Water vapour and carbon dioxide evolved at 140 and 680 °C, which was from the content of $CaC_2O_4•H_2O$ and $CaCO_3$, respectively. In Fig. S8(d) (ESI†), a sharp exothermic peak at 494 °C indicated that the oxidation of carbon and carbon monoxide were released from the CaC_2O_4. The two endothermic peaks at 176 and 817 °C represented the evolution of water molecule from $CaC_2O_4•H_2O$ and the thermal decomposition of $CaCO_3$, respectively.

The morphology and phase evolution of the synthesized adsorbents as a function of NaOH concentration based on the aforementioned results are presented in Fig. 4. Firstly, in the sol–gel process, the citrate anion $(C_6H_5O_7)^{3-}$ is presumed to combine with the calcium ion Ca^{2+} to form calcium–citric acid chelate complexes during the gelation of sol. Afterwards, the dry gel was dissolved by adding different concentrations of NaOH solution. In this process, some of the OH^- ions in the solution might neutralize the H^+ ions derived from the citric acid, while other OH^- ions might react with the Ca^{2+}–citric acid chelate complexes. During the hydrothermal reaction, decomposition of citric acid would take place and subsequently produce carbonate ions CO_3^{2-} in the aqueous solution. Therefore, at a low concentration of NaOH (2 M), three different ionic species (Ca^{2+}, OH^- and CO_3^{2-}) were available as reactants. At these conditions, Ca^{2+}–citric acid chelate complexes would preferably react with CO_3^{2-} to form $CaCO_3$ because the free energy formation of $CaCO_3$ are -1129.1, which is lower than that of calcium hydroxide (-897.5). Once the entire CO_3^{2-} ions were consumed for the formation of $CaCO_3$, the rest of the Ca^{2+} in the citric acid chelate complexes would react with OH^- to form $Ca(OH)_2$. This may represent the results obtained at 6 M which showed that the as–prepared particles were dominantly $Ca(OH)_2$. As the number of nanoparticles increased, the total surface energy of the nanoparticles in the solution increased accordingly, and the $Ca(OH)_2$ nanoparticles aggregated to form the hexagonal and rectangular shaped microstructures. When the concentration of NaOH was increased to 10 M, high excess of OH^- ions would react with Ca^{2+}–citric acid chelate complexes in the solution to form the $CaC_2O_4•H_2O$ nanoparticles. The $CaC_2O_4•H_2O$ nanoparticles would then grow into the irregular nanoplates in the solution through oriented aggregation.[55] The irregular nanoplates coalesced with each other through side–by–side means to enlarge the planar area thus forming microplates.

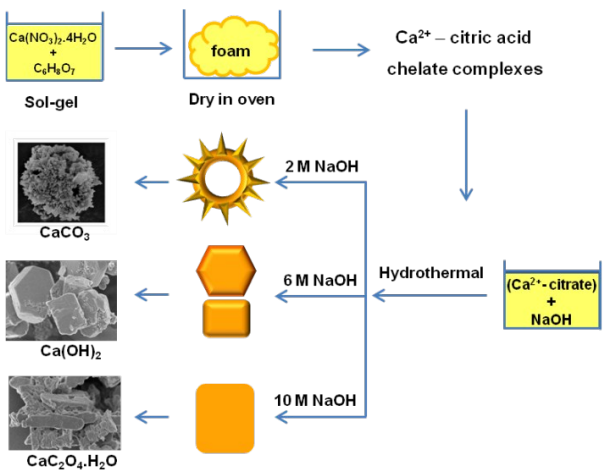

Fig. 4 A schematic diagram of the morphology and phase evolution of the synthesized adsorbents as a function of NaOH concentration.

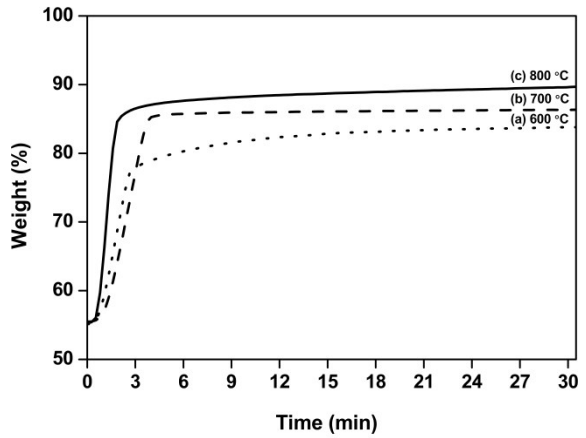

Fig. 5 Effect of temperature on the carbonation of 3D hierarchical $CaCO_3$ hollow microspherical adsorbent composed of 1D spike–shaped nanorods.

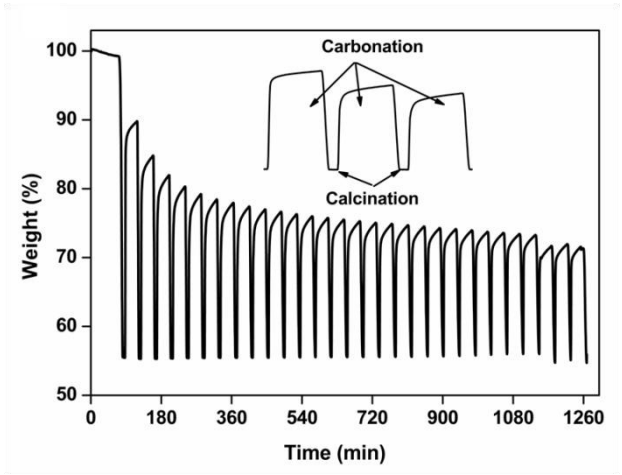

Fig. 6 Weight change associated with 29 carbonation/calcination cycles of 3D hierarchical $CaCO_3$ hollow microspherical adsorbent composed of 1D spike–shaped nanorods.

3.3 CO_2 adsorption analysis

To investigate the effect of temperature on the carbonation of $CaCO_3$ hollow microspheres adsorbent, a set of experiment was conducted at temperature ranging from 600 to 800 °C (Fig. 5). It could be seen that the curves evolved into a plateau stage within 6 min after the carbonation started and the adsorbent achieved over 80% weight gain. The results showed that the $CaCO_3$ hollow microspheres possessed high carbonation rate, which offered a great chance for this adsorbent in practical application. The fast carbonation could be attributed to the larger BET surface area, micro–pore and meso–pore size distributions of the $CaCO_3$ hollow microspherical adsorbent. After 30 min carbonation, the maximum weight gain of the adsorbent at 600, 700 and 800 °C were 84%, 86% and 89%, respectively. It was observed that the maximum weight gain of the $CaCO_3$ adsorbent increased with increasing the carbonation temperature. At 800 °C, the carbonation reaction proceeded quickly.

In this study, the carbonation and calcination reactions were carried out at the same temperature (800 °C) in order to avoid the repetitive heating and cooling of the adsorbents between cyclic operations which in turn resulted to reduce the effect of the thermal stress on the adsorbents.[48, 56] Sun et al.[57] and Lysikov et al.[38] reported that the carbonation processes carried out at long carbonation time (up to 30 min) exhibited substantially higher residual conversions than the processes performed at short carbonation time (less than 10 min). In contrast, the effect of calcination time (3–60 min) was only visible for first few cycles and it became modest when the number of cycles was increased.[32, 38] In this experiment, 30 min was selected to perform carbonation reaction to attain substantially higher residual conversions and the calcination time was fixed for 6 min to reduce sintering of the adsorbents for multiple cycles.

Fig. 6 shows the profiles of 29 consecutive carbonation/ calcination cycles of the calcite $CaCO_3$ hollow microspherical adsorbent in percentage weight. The weight gain dropped from 89% of first cycle to 71% after 29 cycles. The detail of the carbonation/calcination profile for 30 and 6 min could be described by equations (3) to (5), respectively. When the as–synthesized $CaCO_3$ adsorbent was heated from room temperature to 800°C under 100% N_2 gas, the thermal decomposition of $CaCO_3$ adsorbent was observed, as expressed in equation (3). Then, the temperature was maintained at 800°C for 6 min to ensure complete decomposition of $CaCO_3$. After that, the reaction atmosphere was switched to a 100% CO_2, the carbonation reaction of CaO took place (equation (4)) to form the carbonated $CaCO_3$. This step was followed by the calcination reaction (equation (5)) whereby the carbonated $CaCO_3$ converted to CaO under 100% N_2 gas.

$$CaCO_{3\,(as-synthesized)} + N_2 \xrightarrow{800\,^{\circ}C} CaO + CO_2 + N_2 \quad (3)$$

$$CaO + CO_2 \xrightarrow{800\,^{\circ}C} CaCO_{3\,(carbonated)} \quad (4)$$

$$CaCO_{3\,(carbonated)} + N_2 \xrightarrow{800\,^{\circ}C} CaO + CO_2 + N_2 \quad (5)$$

The carbonation conversion of the $CaCO_3$ adsorbent for multiple cycles is shown in Fig. S9 (ESI†). Notably, the maximum conversion of 79% was achieved after 30 min carbonation in the 1st cycle compared with 38% following the 29th cycle. The carbonation reaction appeared in the two–stages. The initial reaction (chemical controlled reaction) stage was completed within the first 2 min due to the rapid surface reaction between CO_2 and CaO to form the $CaCO_3$ product layer covering the CaO core.[58] The higher conversion in the first cycle was due to the extent of conversion attained during the chemical controlled reaction stage. In the second stage (diffusion controlled reaction, 2–30 min), CO_2 diffused through a layer of nascent $CaCO_3$ to react with the unconverted CaO core.[59] A sharp decay in the carbonation conversion occurred during the first five cycles and thereafter became sluggish. The former condition was due to the loss of pore volume of the adsorbent whereas the latter condition was caused by the sintering effect.[60] On the other hand, the increase in grain size [61] and the collapse of morphology during multiple cycles also affected the degradation of the adsorbent [62] and would be discussed by FESEM images.

Fig. 7 shows the selected carbonation conversion curves (1st and 15th cycle) of the synthesized $CaCO_3$, $Ca(OH)_2$, $CaC_2O_4{\bullet}H_2O$ adsorbents and commercial limestone. For the

initial stage (chemical controlled reaction), the conversion of the hollow sphere $CaCO_3$ adsorbent completed about 67% while $Ca(OH)_2$, $CaC_2O_4•H_2O$ and limestone attained about 60%, 55% and 65%, respectively. The $CaCO_3$, $CaC_2O_4•H_2O$ adsorbents and limestone completed the initial stage within 2 min, however the $Ca(OH)_2$ adsorbent completed around 3 min. After this stage, the carbonation conversion increased relatively slow with time. Notably, the increase in conversion of $CaCO_3$, $CaC_2O_4•H_2O$ adsorbents and limestone were about 12% in the second stage (diffusion controlled reaction), however, the conversion for $Ca(OH)_2$ adsorbent increased to about 30%. After 30 min carbonation, the carbonation conversion achieved 79%, 94%, 68% and 77% for $CaCO_3$, $Ca(OH)_2$, $CaC_2O_4•H_2O$ adsorbents and limestone, respectively.

The difference in carbonation conversion between the adsorbents might be caused by the variance in the nucleation rate of $CaCO_3$.[63] The conversion of the adsorbents in the first cycle was ranked as follows: $Ca(OH)_2$ > $CaCO_3$ > limestone > $CaC_2O_4•H_2O$. However, after the 15th cycle, the ranking of the conversion changed to be $CaCO_3$ > $CaC_2O_4•H_2O$ > limestone > $Ca(OH)_2$. The decaying carbonation conversion of $CaCO_3$, $Ca(OH)_2$, $CaC_2O_4•H_2O$ adsorbents and limestone after multiple cycles were attributed to the growth of crystallite of the CaO particle due to the sintering accompanied by the calcination process. The growth of crystallite results to a decrease in reactive surface area, which consequently decreased the overall reaction rate.[64] In addition, the different carbonation conversions of the $CaCO_3$, $Ca(OH)_2$, $CaC_2O_4•H_2O$ adsorbents and limestone could be due to the different morphologies and BET surface areas of the adsorbents. Lu et al.[65] and Gupta and Fan[36] assumed that the differences in reactivity appeared due to the differences in the adsorbent morphology and not because of a reflection of chemistry of the gas−solid reaction that took place on the CaO surface, as all of the CaO adsorbents which obtained from different precursors showed similar crystal structure.

In this study, the mass of the adsorbents tested in multi cycles TG experiments was not sufficiently high to perform the physisorption analysis. Through the observation with SEM, Lu et at. found that pore volumes and surface areas of the adsorbents were based on their different morphologies, which finally determined their carbonation performances.[48] Hence, the FESEM analysis was used to investigate the sintering effect on the morphologies of the adsorbents after multiple carbonation/ calcination cycles. As shown in Fig. S10(a) (ESI†), the spike−shaped $CaCO_3$ nanorods merged into interconnected networks after 1 cycle, however, the hollow structure still occurred. As shown in Fig. S10(b) (ESI†)), the hollow structure disappeared after 29 cycles and a noticeable increase in grain size could be observed. The increase in CaO grain size with number of cycles could be affected the CO_2 adsorption performance for subsequent cycles.[61] The FESEM images in Fig. S10 (ESI†) indicated a change in pore structure. After 1 cycle, the adsorbent exhibited small pores (40−70 nm), whereas after 29 cycles, small pores almost disappeared and larger pores (~700 nm) were observed. The increase in grains size, change in pore structure, the appearance of agglomerates and smooth surface were the typical of the sintering effect, led to the lower surface area,[61, 67, 68] which in turn resulted to a decrease in carbonation conversion of the $CaCO_3$ adsorbent.

Fig. S11 (ESI†) shows FESEM images of $Ca(OH)_2$, $CaC_2O_4•H_2O$ and limestone after 15 cycles. As seen in FESEM images, there were two different types of textures on the surface of the $Ca(OH)_2$ and $CaC_2O_4•H_2O$ adsorbents, while the limestone showed cracks in the CaO crystalline structure as reported in literature.[69] As shown in Fig. S11(a) and (b) (ESI†), one texture was a large number of smaller CaO grains appeared to agglomerate together. The other texture was a compact solid with smooth surface, which covered the agglomerated CaO grains in some area. These two textures might be decreased the CO_2 reaction rate because there were very few pores available for gas-solid reaction and CO_2 had to penetrate the agglomerated grain during carbonation reaction. The FESEM results demonstrated that $Ca(OH)_2$ and $CaC_2O_4•H_2O$ adsorbents experienced serious sintering effect, which led to obviously reduce the surface area and CO_2 adsorption performances.[70]

The cyclic carbonation conversions of the synthesized adsorbents under different NaOH concentrations are presented in Fig. 8. For comparison purposes, the solid line calculated from a

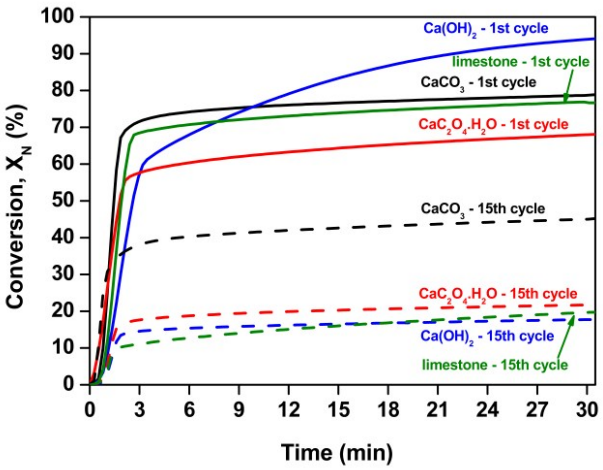

Fig. 7 The 1st and 15th carbonation conversion curves of $CaCO_3$, $Ca(OH)_2$, $CaC_2O_4.H_2O$ adsorbents and limestone.

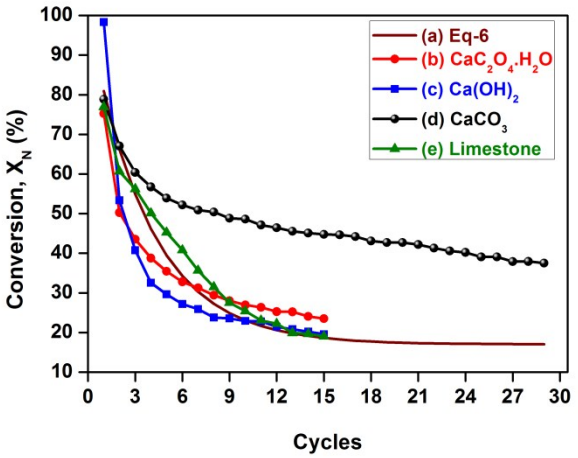

Fig. 8 Cyclic carbonation conversions of $CaCO_3$, $Ca(OH)_2$, $CaC_2O_4.H_2O$ adsorbents and limestone.

Cite this: DOI: 10.1039/c0xx00000x

www.rsc.org/xxxxxx

ARTICLE TYPE

Table 2 Summary of the carbonation conversions of $CaCO_3$ adsorbents and limestone.

Adsorbents	Morphology	Temperature (°C)		Time (min)		Cycles (n)	Conversion (%)	Ref
		Carbonation	Calcination	Carbonation	Calcination			
$CaCO_3$ (synthesized)	hollow microsphere	800	800	30	6	29	~ 38	this study
$CaCO_3$ (synthesized)	spherical shaped mixed with cubic shaped	800	800	30	7.5	29	~ 30	38
$CaCO_3$ (synthesized)	porous sphere shaped	650	700	45	30	18	~ 31	39
$CaCO_3$ (synthesized)	nanopod	750	750	20	20	29	~ 30	37
$CaCO_3$ (commercial)	-	600	700	20	20	29	~ 30	37
$CaCO_3$ (commercial)	nanoparticle	650	850	20	20	29	~ 30	66
Havelock (limestone)	-	650	850	10	10	29	~ 20	32
Cadomin (limestone)	-	650	850	10	10	29	~ 20	32
Blanca (limestone)	-	650	850	10	10	29	~ 20	32
Piasek (limestone)	-	650	850	10	10	29	~ 20	32
Gotland (limestone)	-	650	850	10	10	29	< 20	32
La Blanca (limestone)	-	650	850	20	20	29	< 20	32
Strassburg (limestone)	-	850	850	9	8	29	< 20	57

semi–empirical model that was proposed for the decay of the capture capacity by Abanades and Alvarez [69] was attached (equation (6)),

$$X_N = f_m^N(1 - f_w) + f_w \quad (6)$$

where X_N is the maximum carbonation conversion achieved after N cycles, $f_m = 0.77$ and $f_w = 0.17$. After 15 cycles, the carbonation conversion of $CaCO_3$ hollow microspheres was 45%, which was about 22% higher than the semi–empirical model, CaC_2O_4•H_2O, $Ca(OH)_2$ adsorbents and limestone. In comparison, the residual conversion ~ 38% for $CaCO_3$ hollow microspheres after 29 cycles was higher than those of spherical shaped mixed with cubic shaped $CaCO_3$ adsorbent, $CaCO_3$ nanopod, commercial $CaCO_3$ adsorbents and natural limestone reported in literatures as summarized in Table 2.[32, 37-39, 57, 66] This finding means that the hierarchical $CaCO_3$ hollow microspheres composed of spike–shaped nanorod adsorbent possessed better anti–sintering performances than others CaO–based adsorbents. This may be attributed to the novel 3D structure, which has larger surface area and the trimodal pore size distribution (micro–pore and meso–pore range). This structure enhanced the performance of the CO_2 adsorption for multiple carbonation/calcination cycles and could be the potential adsorbents structure for CO_2 capture.

4. Conclusions

We successfully synthesized the novel microstructured hierarchical calcite $CaCO_3$ hollow spherical adsorbent composed of spike–shaped nanorods by the sol–gel hydrothermal with varying NaOH concentrations. This is a new proposed approach to prepare 3D hierarchical calcite $CaCO_3$ hollow microspheres without surfactants. The hierarchical $CaCO_3$ hollow microspheres produced at 2 M NaOH exhibited the best CO_2 adsorption performances, which was about 22% higher than that of $Ca(OH)_2$ and CaC_2O_4•H_2O adsorbents synthesized with 6 and 10 M NaOH. This is attributed to the 3D hierarchical hollow microsphere structure, 1D spike–shaped nanorod structure, large BET surface area and trimodal pore size distribution. The enhanced performance of the novel morphology indicated that it is a promising adsorbent for CO_2 adsorption and a potential candidate for other applications, such as catalysis, filler, coating pigment and anticancer drug carrier.

Acknowledgements

The authors thank the AUN/SEED Net Project under grant no. 304/6050219, RU grant no. 814154, Japan International Cooperation Agency (JICA) and Long Term Research Grant (LRGS) (203/PKT/6723001) from the Ministry of Higher Education (MOHE) Malaysia for their financial support. The authors thank Mr. Jon Koki, Technical Department, Center for Advanced Materials Analysis, Tokyo Institute of Technology, for FESEM analysis. The authors also greatly acknowledge the Universiti Sains Malaysia and Tokyo Institute of Technology for the use of their facilities.

Notes and references

[a] *School of Materials and Mineral Resources Engineering, Engineering Campus, Universiti Sains Malaysia, 14300 Nibong Tebal, Penang, Malaysia. Fax: +60-604 5995215; Tel: +60-6045941011; E-mail: srimala@usm.my, nwenihlaing76@gmail.com*

[b] *Department of International Development Engineering, Tokyo Institute of Technology, 2-12-1 Ookayama, Meguro-ku, Tokyo, Japan, Fax: +81-3-5734-3245; Tel: +81-3-5734-3245; E-mail: hinode@ide.titech.ac.jp*

[c] *Department of Physics, University of Yangon, 11041 Kamayut, Yangon, Myanmar.*

[d] *Low Carbon Economy (LCE) Research Group, School of Chemical Engineering, Engineering Campus,Universiti Sains Malaysia, 14300 Nibong Tebal, Penang, Malaysia.*

[e] *Environmental Engineering, Surya University, Tangerang, 15810 Banten, Indonesia.*

† Electronic Supplementary Information (ESI) available: [XRD pattern of limestone, FTIR spectrum, EDX spectrum and TG–DTA curves of 3D hierarchical $CaCO_3$ hollow microspherical adsorbent, FESEM image of

the commercial limestone, FTIR spectra, EDX spectra, TG and DTA curves of $Ca(OH)_2$ and $CaC_2O4.H_2O$ adsorbents, Multi cycles carbonation conversion curves of 3D hierarchical calcite $CaCO_3$ hollow microspherical adsorbent, FESEM images of the adsorbents after multiple cycles, BET surface area and crystallite sizes of synthesized adsorbents under different NaOH concentrations and TG data of $Ca(OH)_2$ and $CaC_2O4•H_2O$ adsorbents.]. See DOI: 10.1039/b000000x/

1. X. W. Lou, L. A. Archer and Z. Yang, *Advanced Materials*, 2008, **20**, 3987-4019.
2. M. Chen, C. Ye, S. Zhou and L. Wu, *Advanced Materials*, 2013, **25**, 5343-5351.
3. J. Hu, M. Chen, X. Fang and L. Wu, *Chemical Society Reviews*, 2011, **40**, 5472-5491.
4. H. Dong, Y. Liu, G. Li, X. Wang, D. Xu, Z. Chen, T. Zhang, J. Wang and L. Zhang, *Sensors and Actuators B: Chemical*, 2013, **178**, 302-309.
5. S. Ding and X. Wen Lou, *Nanoscale*, 2011, **3**, 3586-3588.
6. S.-D. Jiang, Q.-Z. Yao, G.-T. Zhou and S.-Q. Fu, *The Journal of Physical Chemistry C*, 2012, **116**, 4484-4492.
7. A.-M. Cao, J.-S. Hu, H.-P. Liang and L.-J. Wan, *Angewandte Chemie International Edition*, 2005, **44**, 4391-4395.
8. L.-P. Zhu, G.-H. Liao, Y. Yang, H.-M. Xiao, J.-F. Wang and S.-Y. Fu, *Nanoscale research letters*, 2009, **4**, 550-557.
9. Z. Sun, T. Liao, K. Liu, L. Jiang, J. H. Kim and S. X. Dou, *Nano Research*, 2013, **6**, 726-735.
10. Z. Bian, J. Zhu, J. Wang, S. Xiao, C. Nuckolls and H. Li, *Journal of the American Chemical Society*, 2012, **134**, 2325-2331.
11. J. B. Fei, Y. Cui, X. H. Yan, W. Qi, Y. Yang, K. W. Wang, Q. He and J. B. Li, *Advanced Materials*, 2008, **20**, 452-456.
12. X. Guan, L. Li, G. Li, Z. Fu, J. Zheng and T. Yan, *Journal of Alloys and Compounds*, 2011, **509**, 3367-3374.
13. B. Wang, J. S. Chen, H. B. Wu, Z. Wang and X. W. Lou, *Journal of the American Chemical Society*, 2011, **133**, 17146-17148.
14. L. Zhao and J. Wang, *Colloids and Surfaces A: Physicochemical and Engineering Aspects*, 2012, **393**, 139-143.
15. W. Dong, H. Cheng, Y. Yao, Y. Zhou, G. Tong, D. Yan, Y. Lai and W. Li, *Langmuir*, 2010, **27**, 366-370.
16. M. F. Butler, W. J. Frith, C. Rawlins, A. C. Weaver and M. Heppenstall-Butler, *Crystal Growth & Design*, 2008, **9**, 534-545.
17. W. Wei, G.-H. Ma, G. Hu, D. Yu, T. McLeish, Z.-G. Su and Z.-Y. Shen, *Journal of the American Chemical Society*, 2008, **130**, 15808-15810.
18. L. Qi, J. Li and J. Ma, *Advanced Materials*, 2002, **14**, 300-303.
19. T. Enomae and K. Tsujino, *Appita J*, 2004, **57**, 493-493.
20. Y. Guan, X. Meng and D. Qiu, *Langmuir*, 2014, **30**, 3681-3686.
21. M. Wan, *Advanced Materials*, 2008, **20**, 2926-2932.
22. L. Y. Xia, M. Q. Zhang, C. e. Yuan and M. Z. Rong, *Journal of Materials Chemistry*, 2011, **21**, 9020-9026.
23. S. P. Gopi, P. Vijaya and V. K. Subramanian, *Powder Technology*, 2012, **225**, 58-64.
24. I. Lee, H. Han and S.-Y. Lee, *Journal of Crystal Growth*, 2010, **312**, 1741-1746.
25. D. Zhao, J. Jiang, J. Xu, L. Yang, T. Song and P. Zhang, *Materials Letters*, 2013, **104**, 28-30.
26. Y. Wang, Y. X. Moo, C. Chen, P. Gunawan and R. Xu, *Journal of Colloid and Interface Science*, 2010, **352**, 393-400.
27. S. Choi, J. H. Drese and C. W. Jones, *ChemSusChem*, 2009, **2**, 796.
28. M. Afkhamipour and M. Mofarahi, *International Journal of Greenhouse Gas Control*, 2014, **25**, 9-22.
29. C.-H. Yu, C.-H. Huang and C.-S. Tan, *Aerosol and Air Quality Research*, 2012, **12**, 745-769.
30. P. Sun, J. R. Grace, C. J. Lim and E. J. Anthony, *AIChE Journal*, 2007, **53**, 2432-2442.
31. J. C. Abanades, E. J. Anthony, D. Y. Lu, C. Salvador and D. Alvarez, *AIChE Journal*, 2004, **50**, 1614-1622.
32. G. S. Grasa and J. C. Abanades, *Industrial & Engineering Chemistry Research*, 2006, **45**, 8846-8851.
33. V. Manovic and E. J. Anthony, *Environmental Science & Technology*, 2008, **42**, 4170-4174.
34. Y. J. Li, C. S. Zhao, C. R. Qu, L. B. Duan, Q. Z. Li and C. Liang, *Chemical Engineering & Technology*, 2008, **31**, 237-244.
35. F. Donat, N. H. Florin, E. J. Anthony and P. S. Fennell, *Environmental Science & Technology*, 2011, **46**, 1262-1269.
36. H. Gupta and L.-S. Fan, *Industrial & Engineering Chemistry Research*, 2002, **41**, 4035-4042.
37. Z. Yang, M. Zhao, N. H. Florin and A. T. Harris, *Industrial & Engineering Chemistry Research*, 2009, **48**, 10765-10770.
38. A. I. Lysikov, A. N. Salanov and A. G. Okunev, *Industrial & engineering chemistry research*, 2007, **46**, 4633-4638.
39. S. Wang, L. Fan, C. Li, Y. Zhao and X. Ma, *ACS applied materials & interfaces*, 2014.
40. E. T. Santos, C. Alfonsín, A. J. S. Chambel, A. Fernandes, A. P. Soares Dias, C. I. C. Pinheiro and M. F. Ribeiro, *Fuel*, 2012, **94**, 624-628.
41. M. Ghiasi and A. Malekzadeh, *Crystal Research and Technology*, 2012, **47**, 471-478.
42. S. Gunasekaran, G. Anbalagan and S. Pandi, *Journal of Raman Spectroscopy*, 2006, **37**, 892-899.
43. X. Yang, H. Meng, T. Li, L. Shi, Y. Li and G. Xu, *Powder Technology*, 2014, **256**, 272-278.
44. R. R. Virtudazo, H. Watanabe, T. Shirai, M. Fuji and M. Takahashi, in *IOP Conference Series: Materials Science and Engineering*, IOP Publishing, 2011, p. 062014.
45. K. S. Sing, *Journal of Porous Materials*, 1995, **2**, 5-8.
46. K. S. Sing, *Pure and applied chemistry*, 1985, **57**, 603-619.
47. C. Luo, Q. Shen, N. Ding, Z. Feng, Y. Zheng and C. Zheng, *Chemical Engineering & Technology*, 2012, **35**, 547-554.
48. H. Lu, E. P. Reddy and P. G. Smirniotis, *Industrial & Engineering Chemistry Research*, 2006, **45**, 3944-3949.
49. T. Liu, Y. Zhu, X. Zhang, T. Zhang, T. Zhang and X. Li, *Materials Letters*, 2010, **64**, 2575-2577.
50. J.-M. Ouyang, H. Zheng and S.-P. Deng, *Journal of Crystal Growth*, 2006, **293**, 118-123.
51. I. Petrov and B. Šoptrajanov, *Spectrochimica Acta Part A: Molecular Spectroscopy*, 1975, **31**, 309-316.
52. S. J. Palmer, M. K. Smith and R. L. Frost, *Journal of Industrial and Engineering Chemistry*, 2011, **17**, 56-61.
53. S. Chedella and D. Berzins, *International endodontic journal*, 2010, **43**, 509-518.
54. R. L. Frost and M. L. Weier, *Thermochimica Acta*, 2004, **409**, 79-85.
55. Y. Cheng, Y. Wang, Y. Zheng and Y. Qin, *The Journal of Physical Chemistry B*, 2005, **109**, 11548-11551.
56. V. Manovic and E. J. Anthony, *Energy & Fuels*, 2008, **22**, 1851-1857.
57. P. Sun, C. J. Lim and J. R. Grace, *AIChE journal*, 2008, **54**, 1668-1677.
58. T. Witoon, *Ceramics International*, 2011, **37**, 3291-3298.
59. A. Akgsornpeak, T. Witoon, T. Mungcharoen and J. Limtrakul, *Chemical Engineering Journal*, 2014, **237**, 189-198.
60. R. Barker, *Journal of Applied Chemistry and Biotechnology*, 1974, **24**, 221-227.
61. Y. Zhu, S. Wu and X. Wang, *Chemical Engineering Journal*, 2011, **175**, 512-518.
62. C. Zhao, Z. Zhou and Z. Cheng, *Industrial & Engineering Chemistry Research*, 2014, **53**, 14065-14074.
63. W. Liu, N. W. Low, B. Feng, G. Wang and J. C. Diniz da Costa, *Environmental science & technology*, 2009, **44**, 841-847.
64. B. Feng, H. An and E. Tan, *Energy & Fuels*, 2007, **21**, 426-434.
65. H. Lu, A. Khan and P. G. Smirniotis, *Industrial & Engineering Chemistry Research*, 2008, **47**, 6216-6220.
66. N. H. Florin and A. T. Harris, *Chemical Engineering Science*, 2009, **64**, 187-191.

67. D. Alvarez and J. C. Abanades, *Industrial & Engineering Chemistry Research*, 2005, **44**, 5608-5615.
68. C. Luo, Y. Zheng, N. Ding, Q. Wu, G. Bian and C. Zheng, *Industrial & Engineering Chemistry Research*, 2010, **49**, 11778-11784.
69. J. C. Abanades and D. Alvarez, *Energy & Fuels*, 2003, **17**, 308-315.
70. Z.-s. Li, N.-s. Cai and Y.-y. Huang, *Industrial & Engineering Chemistry Research*, 2006, **45**, 1911-1917.